CHAPTER 4

STRESS CONCENTRATION DUE TO SHEAR LAG IN CONTINUOUS BOX GIRDERS

4.1 Introduction

Although normal stress in the longitudinal direction produced by bending deformation is assumed to be uniform across flange width in the elementary beam theory, it is not so in reality if the flange width is large. This phenomenon, known as the shear lag, has been studied for many years. A concise but excellent literature review of research on the shear lag is available in Tenchev (1996). Even in recent years, the subject has attracted many researchers and quite a few researches have been studied.

Continuous girders are quite common structures in practice. Engineers dealing with ordinary box girders for highway bridges and buildings need not be daunted by the stress concentration due to shear lag. However, there are indeed some special cases of short stocky members, so that design codes provide formulas to account for the shear lag effect. Nevertheless, there appears to be very few research results available in the literature on the shear lag effect of continuous girders. Besides, Japan (2002) and Eurocode 3 (2003) yield very different shear lag effects, which will be shown later in this chapter.

Against the background of the above information, the three-dimensional finite element analysis of a continuous box girder by shell elements is carried out to investigate stress concentration due to the shear lag in the present study. With the multimesh extrapolation method (Cook et al., 1989), the analysis is performed to produce reliable numerical results. An extensive parametric study is conducted and empirical formulas are proposed to deal with the shear lag phenomenon in continuous box girders. In all the analyses, a well-known finite element program, MARC (1994), is used.

4.2 Parametric Study

Three-span continuous box girders under uniformly distributed load are analyzed. The symbols employed in the present study for describing the structural geometry are illustrated in Figure 4.1. For the design of a continuous girder, the stress distributions in the cross sections under large bending moment are important. Therefore, in the present study we focus on three cross sections of Sections A to C shown in Figure 4.1 (b): Section A is under the largest bending moment in the exterior span, Section B is at the interior support (under the largest negative bending moment) and Section C is at the center of the girder, which is under the largest bending moment in the interior span. Following Lertsima et al. (2004), uniformly distributed load is applied as a line load along the centerline of the web as shown in Figure 4.1 (c). Due to symmetry, only a quarter of the girder (a half of the cross section and a half of the girder length) needs be analyzed. Therefore, the symmetric conditions, i.e., no displacement in y-axis and no rotations about x- and z-axes, are imposed on

Section C, while only the displacement in z-axis is suppressed at the end of the girder and Section B. The material property is assumed to be isotropic linear elastic with Young's modulus 206 GPa and Poisson's ratio 0.3.

Three-dimensional finite element analysis is conducted so as to reveal the influence of the parameters that characterize the geometry of a continuous box girder. To this end, the following values are considered: B/H = 0.5, 1.0, 1.5, 2.0; H/L = 0.025, 0.05, 0.10, 0.15, 0.20; T_f/T_w = 0.5, 1.0, 1.5, 2.0; α =1.0, 1.25, 1.5. The combination of all these values results in 240 box girders different from each other in geometry. It is noted that for every girder, multiple finite element meshes are used to reduce discretization error by the multimesh extrapolation method.

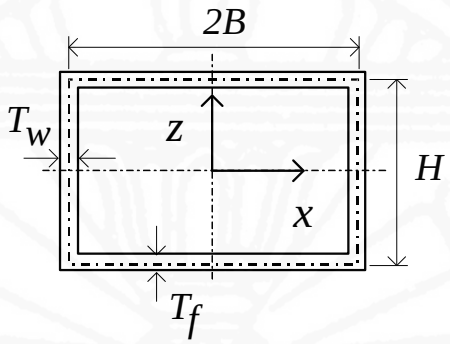

(a) Cross section

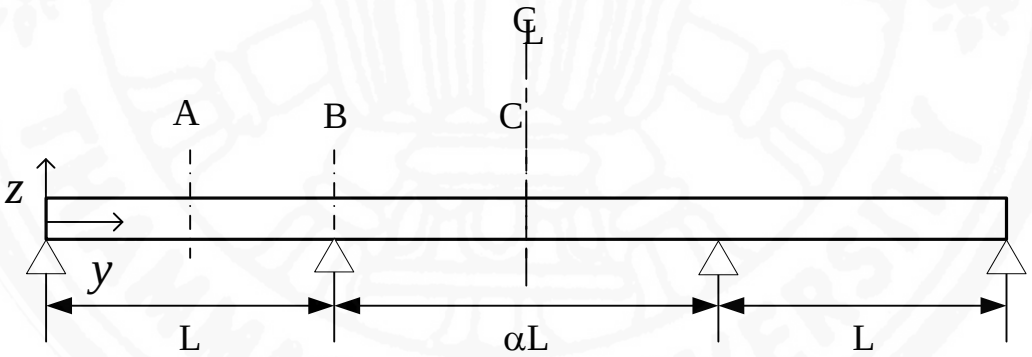

(b) Side view

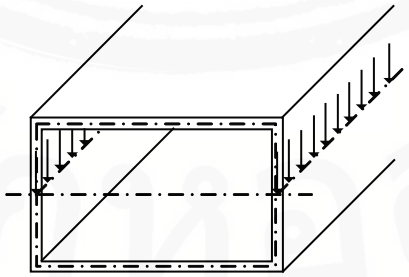

(c) Distributed load

Figure 4.1 Three-span continuous box girder model

The stress concentration factors in Sections A to C can be evaluated by the formula given in the design codes (Japan, 2002; Eurocode 3, 2003). For a box girder with B/H = 2.0, H/L = 0.2, T_f/T_w = 1.0 and α =1.0, those values are computed and presented in Table 4.1, where K_c stands for the stress concentration factor defined by the ratio of the maximum normal stress in the flange to that of the elementary beam theory. Significant discrepancy is recognized, suggesting the necessity of the further study of the shear lag in a continuous girder.

Table 4.1 Comparison of K_c values (H/L=0.2; B/H=2.0; α =1.0; T_f/T_w=1.0)

Literature	K_c		
	Section A	Section B	Section C
Japan (2002)	2.83	4.64	3.51
Eurocode 3 (2003)	2.18	4.74	2.66

4.3 Finite Element Model

In the present study, the continuous box girders are analyzed by three-dimensional finite element method, using 4-node shell elements. In particular, Element 75 (Bilinear Thick Shell Element) is used, and the nodal stress is evaluated as an average of the stresses in the elements sharing the node (MARC, 1994). Although the finite element method is very versatile and powerful, caution must be used since the results may depend largely on the finite element mesh employed in the analysis, which is especially so when stress concentration is dealt with. The dependency on the finite element mesh is attributable to the discretization error. In Lertsima et al. (2004), this issue was looked into numerically, and the multimesh extrapolation method was employed to reduce the discretization error in the evaluation of the stress concentration due to the shear lag. It is noted that the stress concentration factors thus obtained are very close to those obtained by the adaptive finite element method (Lertsima et al., 2004). The multimesh extrapolation method is also used herein, and the numerical procedure is briefly explained in what follows:

Figure 4.2 (a) shows the normal-stress distributions in the upper flange at the mid-span of a simply-supported box girder (B/H =1.0, H/L = 0.2, T_f/T_w = 1.0) that was dealt in Lertsima et al. (2004). In this figure, σ is the normal stress obtained by the three-dimensional finite element analysis, while σ_{beam} is the normal stress due to the elementary beam theory. Needless to say, σ_{beam} is constant across the flange width. Using the 4-node shell elements, four finite element meshes of Meshes A to D are employed herein. All the elements in each mesh are rectangular and every element in the box girder is made quarter in the process of refining the mesh from Meshes A to D: an illustration of Meshes A to D is presented in Figure 4.3. The total numbers of elements are 1,920, 7,680, 30,720 and 122,880 for Meshes A to D, respectively. Figure 4.2 (a) illustrates not only the shear lag phenomenon but also the dependence of the stress distribution on the finite element mesh. As expected, the dependence is stronger at the edge of the flange where the largest stress concentration takes place. At the same time, the tendency of stress convergence is observed, as the size of the finite element becomes smaller.

The stresses at four points in the upper flange obtained by the present finite element analysis are presented in Figure 4.2(b). The figure shows the variation of the normal stress with respect to a representative element size Δ. It is observed that the four lines in Figure 4.2 (b) become almost straight for small Δ. This is in good agreement with the theory that the error in stress is of the order $O(\Delta^p)$ where p is equal to 1 for a bilinear element (Cook et al., 1989; Zienkiewicz, 2005). Therefore, the linear extrapolation illustrated by the dotted lines in Figure 4.2 (b) can be used to estimate the converged stress. This extrapolation method is called the multimesh extrapolation method by Cook et al. (1989) and is applied to the present study. The stress ratio σ/σ_{beam} at the edge of the flange thus obtained, i.e., the point indicated by an arrow in Figue 4.2 (b), is the value of K_c that the authors seek in the present numerical study.

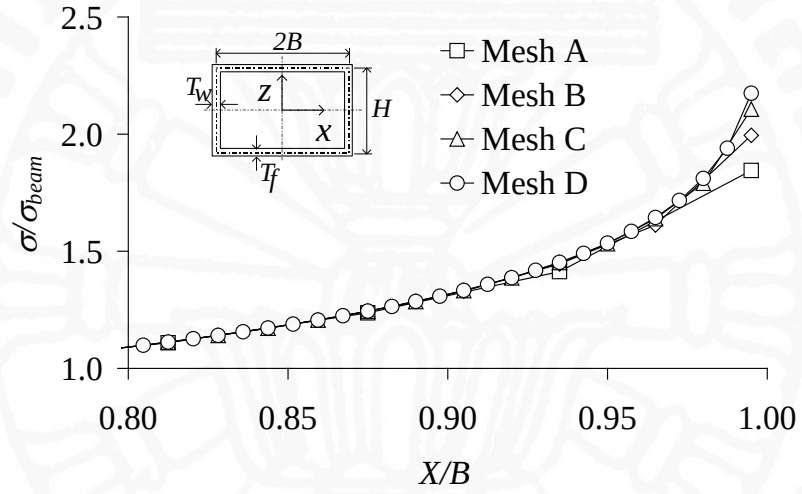

(a) Normal-stress distribution in upper flange

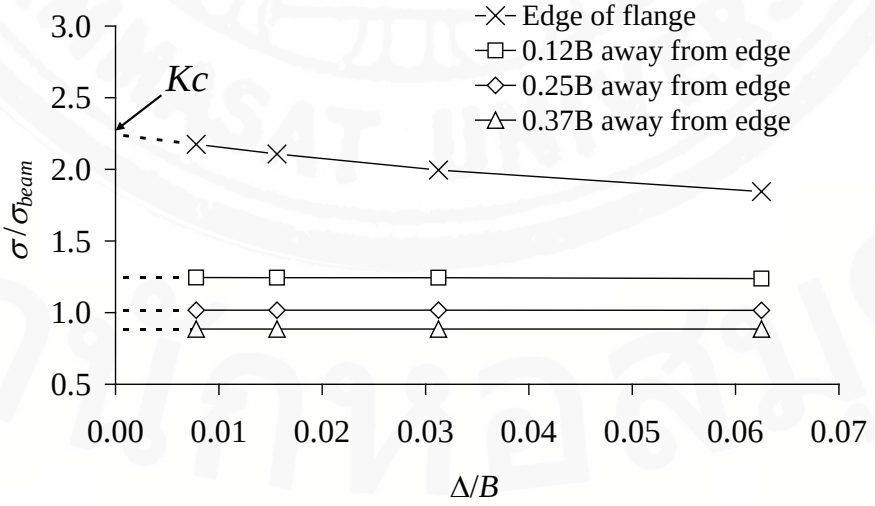

(b) Variation of normal stress with respect to representative element size

Figure 4.2 Dependence of normal stress on finite element mesh

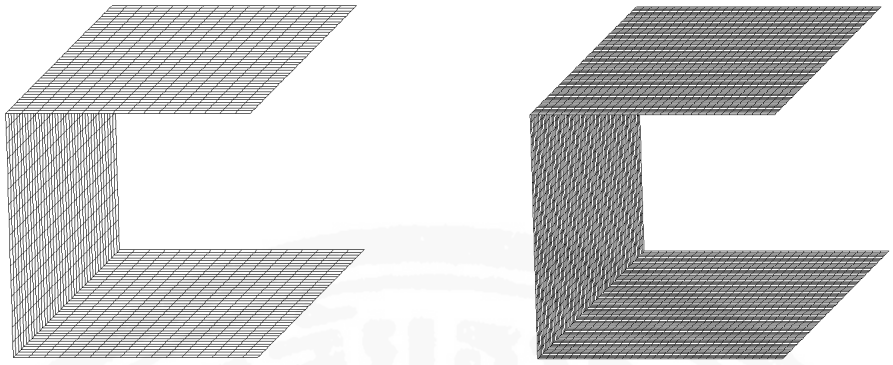

(a) Mesh A (b) Mesh B

(c) Mesh C (d) Mesh D

Figure 4.3 Finite element meshes for a quarter of the box girder

4.4 Normal Stress Distribution in Upper Flange

Figure 4.4 shows two variations of the normal stress at the edge of the upper flange along the length of the girder with B/H=2.0, H/L =0.2, α =1.5 and T_f/T_w =2.0: one is obtained by the elementary beam theory and the other by the finite element analysis (FEA). Due to symmetry, only the stress distribution along a half of the girder (y/L=0.0 - 1.75) is given: y/L=1.75 corresponds to the location of Section C. Note that σ_0 is the stress due to the beam theory at the internal support (Section B). The significant difference between the two normal-stress distributions confirms the importance of the shear lag in a continuous box girder.

The normal-stress distribution in the upper flange of various cross sections is presented in Figure 4.5. The distribution varies considerably from section to section. It may be noteworthy that as can be seen typically in Figures 4.5 (a) and (f), near the mid-span in the exterior span the magnitude of the normal stress decreases towards the center of the flange and the smallest value is nearly equal to zero, while the smallest value is rather close to the normal stress of the beam theory near the mid-span in the interior span. The normal-stress distribution in a simply-supported box girder has been found to be similar to that of the exterior span of the continuous box girder.

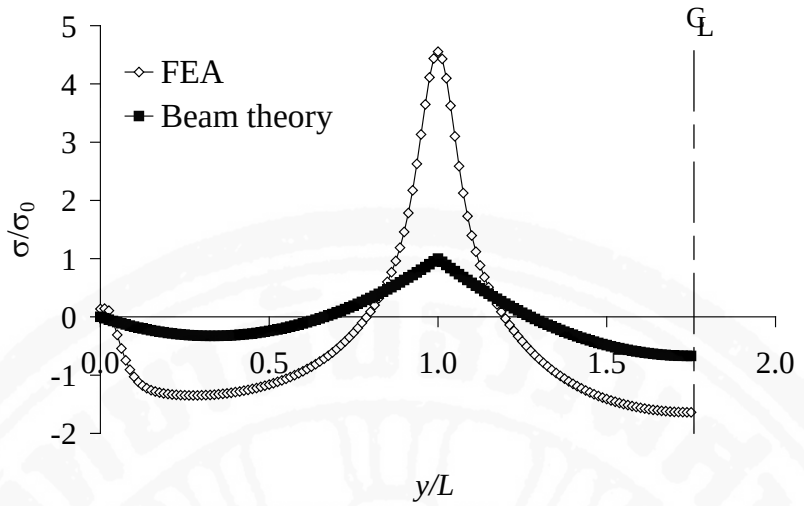

Figure 4.4 Variation of normal stress at edge of upper flange (B/H=2.0; H/L=0.2; T_f/T_w=2.0; α=1.5)

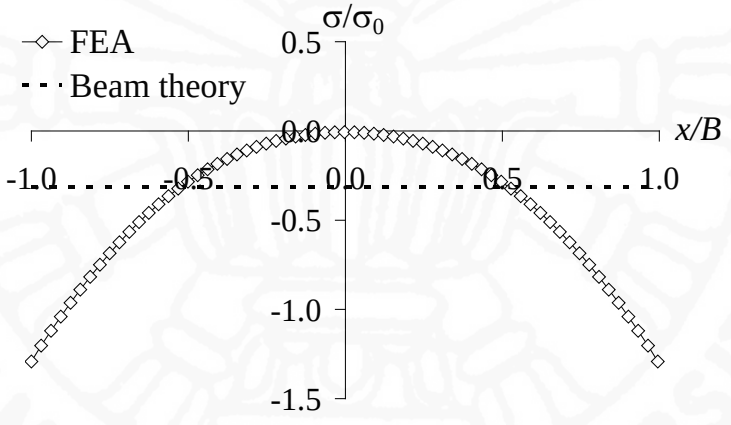

(a) y/L=0.4

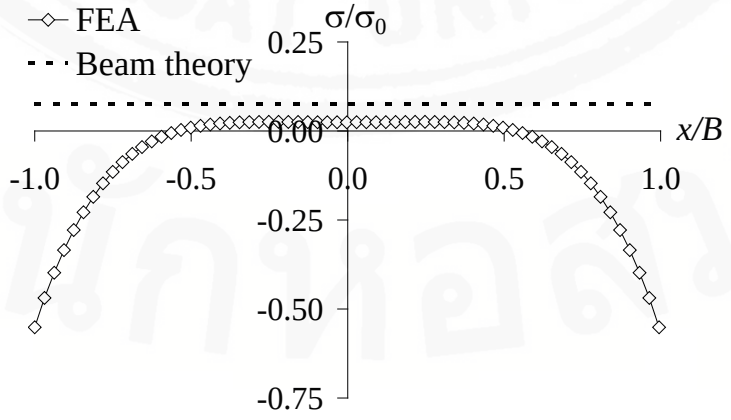

(b) y/L=0.7

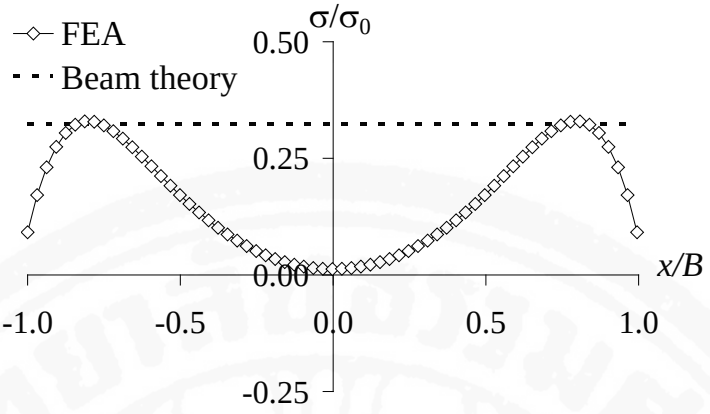

(c) *y/L*=0.8

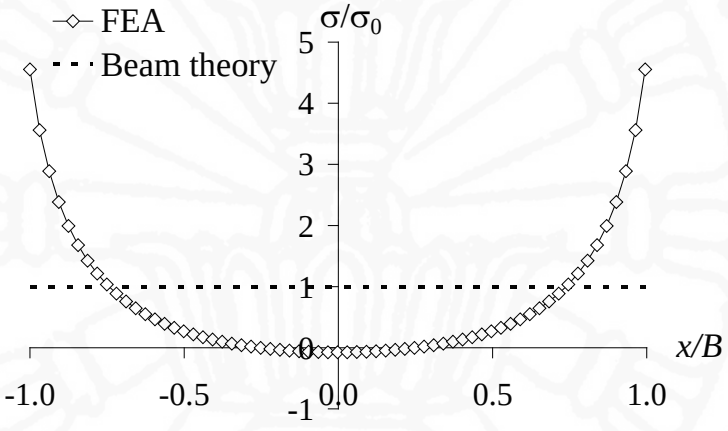

(d) *y/L*=1.0 (Section B)

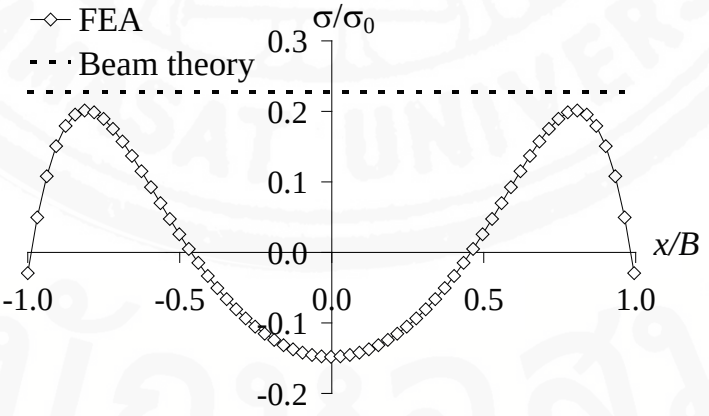

(e) *y/L*=1.2

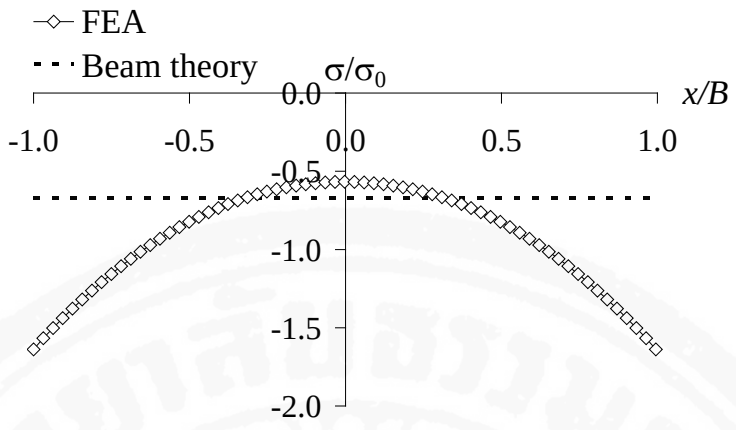

(f) y/L=1.75 (Section C)

Figure 4.5 Normal-stress distribution in upper flange

4.5 Effect of Geometric Property

Typical examples of the present numerical results for Section A are shown in Figure 4.6. The trends of the variation of K_c with respect to the parameters may be summarized as follows:

K_c tends to increase significantly in general with the increase of B/H or H/L. However, for H/L=0.025 and 0.05 or B/H=0.5, K_c remains almost constant and nearly equal to 1.0: the effect of the shear lag is small.

K_c increases also with the increase of T_f/T_w. However, the change of K_c with respect to T_f/T_w is small. Unlike the cases of B/H and H/L, the K_c–T_f/T_w curves are close to straight lines and the slopes of those curves are almost identical regardless of B/H.

The increase of α increases K_c. However, the dependence of K_c on α is rather small although it becomes slightly bigger for large B/H.

As may be seen in Figure 4.7, the variations of K_c for Sections B and C show similar tendencies except the influence of α: unlike in Section A, K_c decreases as α increases. It is also observed that K_c in Section B is the largest in general. However, the difference between K_c values in the three sections varies with α. At $\alpha = 1.25$ and 1.5, Sections A and C have almost identical values of K_c.

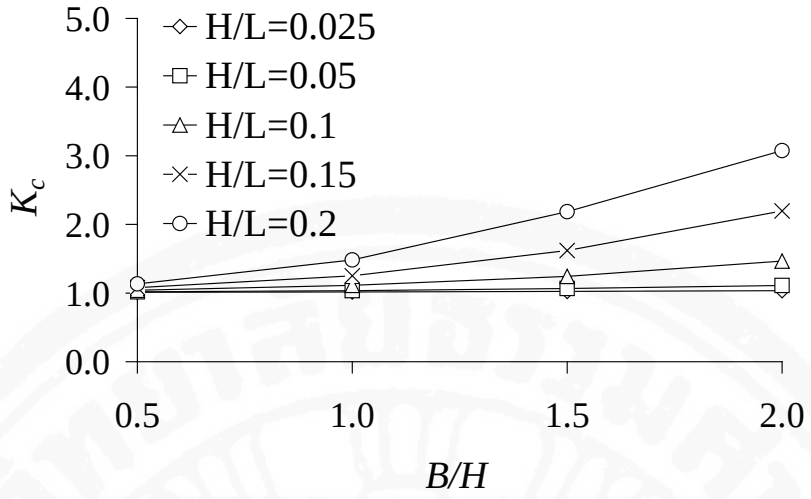

(a) With respect to B/H (T_f/T_w=1.0, α =1.25)

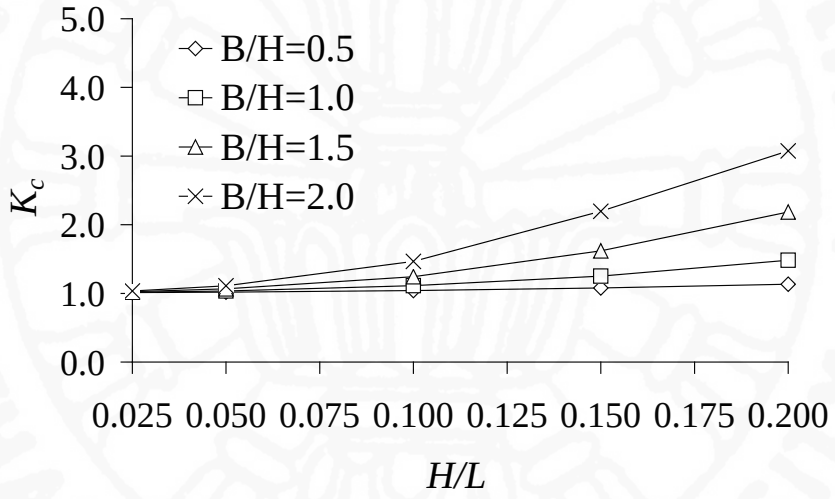

(b) With respect to H/L (T_f/T_w=1.0; α =1.25)

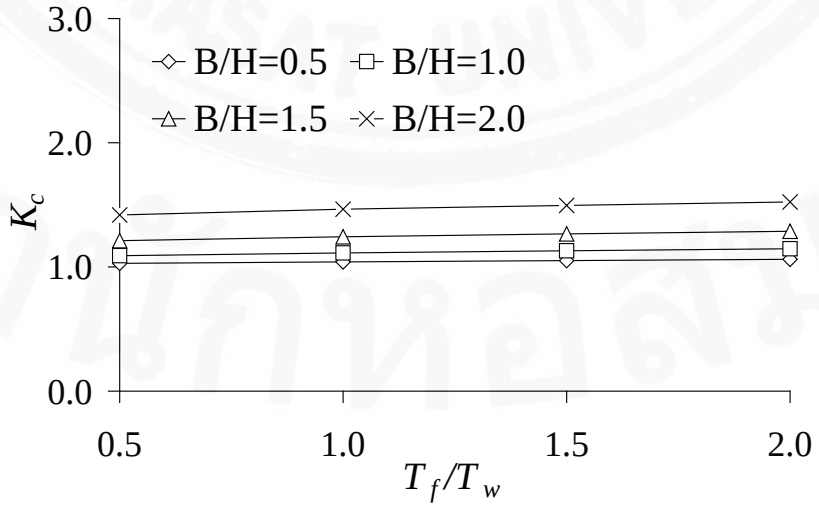

(c) With respect to T_f/T_w (H/L=0.1, α =1.25)

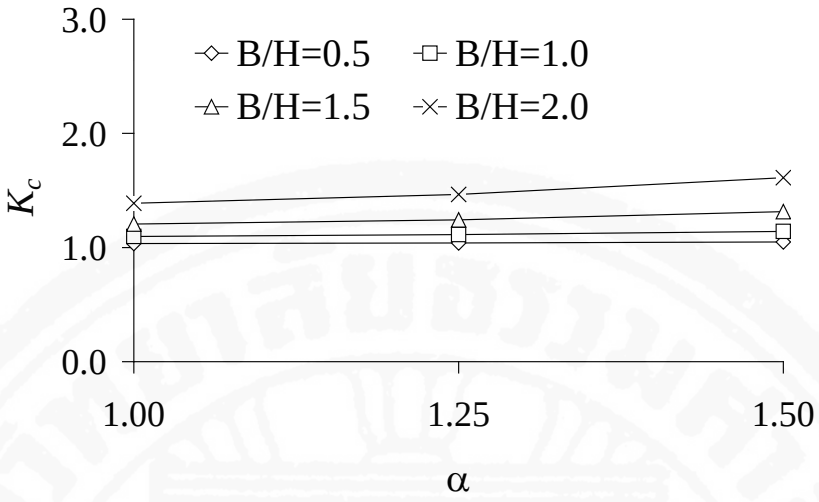

(d) With respect to α (H/L=0.1, T_f/T_w=1.0)

Figure 4.6 Variation of K_c in Section A

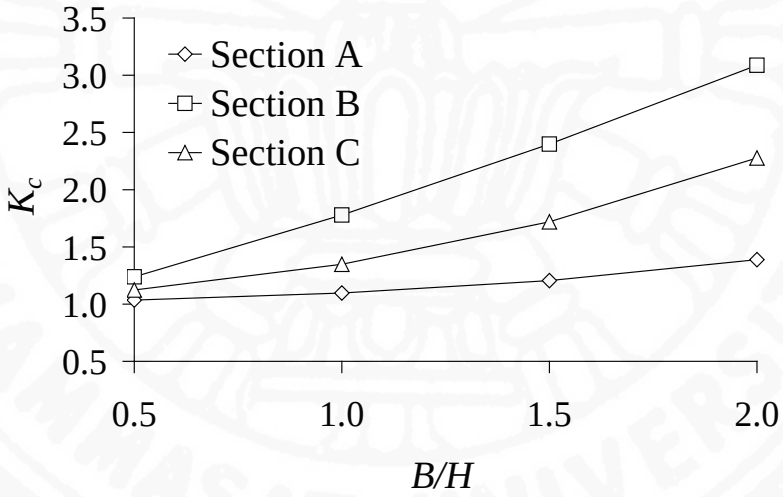

(a) Variation with respect to B/H (H/L=0.1, T_f/T_w=1.0, α =1.0)

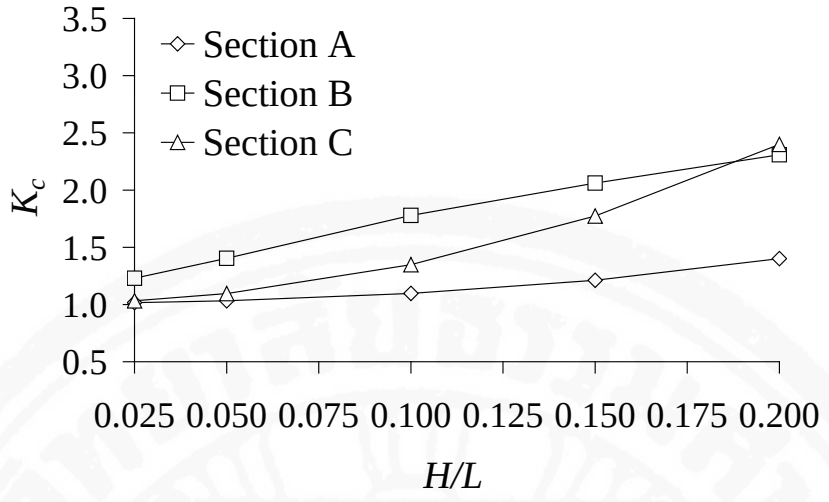

(b) Variation with respect to H/L (B/H=1.0, T_f/T_w=1.0, α =1.0)

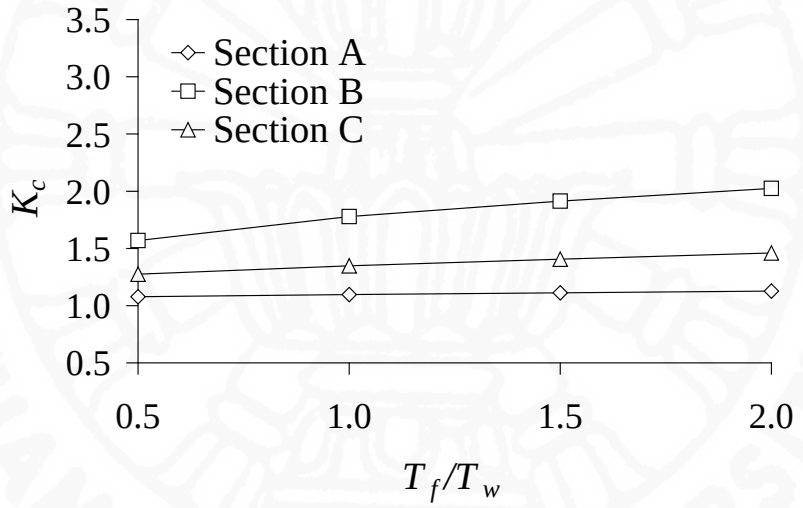

(c) Variation with respect to T_f/T_w (H/L=0.1, B/H=1.0, α =1.0)

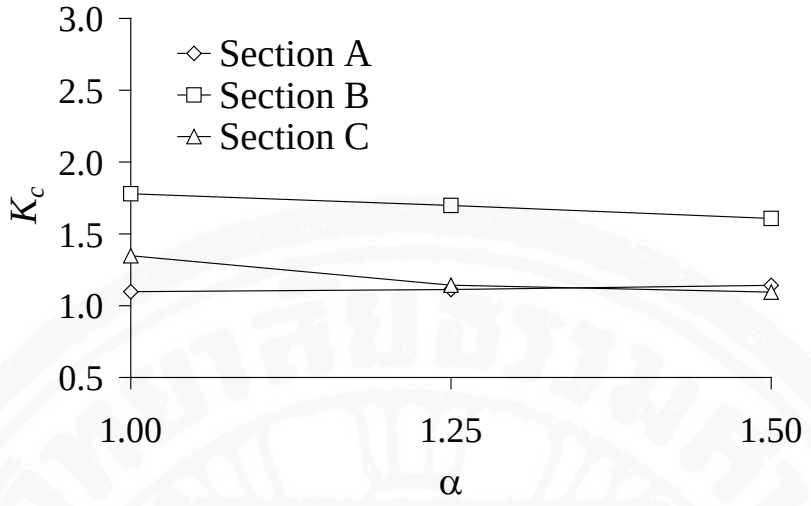

(d) Variation with respect to α (H/L=0.1, B/H=1.0, T_f/T_w=1.0)

Figure 4.7 Comparison of K_c values between cross sections

4.6 Comparison of K_c

Figure 4.8 shows K_c values due to the two design codes (Japan, 2002; Eurocode 3, 2003) together with the present FEA results. The influence of B/H is focused on in particular herein. For Sections A and C, Japan (2002) yields the largest value while Eurocode 3 (2003) gives the smallest. For Section B, the tendency is reversed: K_c due to Eurocode 3 (2003) is consistently larger than that due to Japan (2002). The discrepancy observed in Figure 4.8 is not negligible: it seems rather significant in design practice. Interestingly, the results of the present FEA tend to lie between the two sets of the K_c values due to the two design codes.

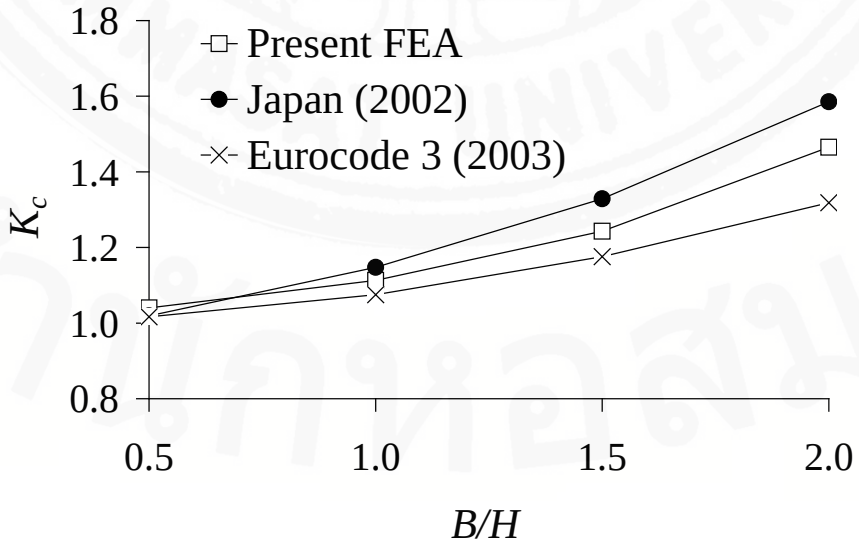

(a) Section A

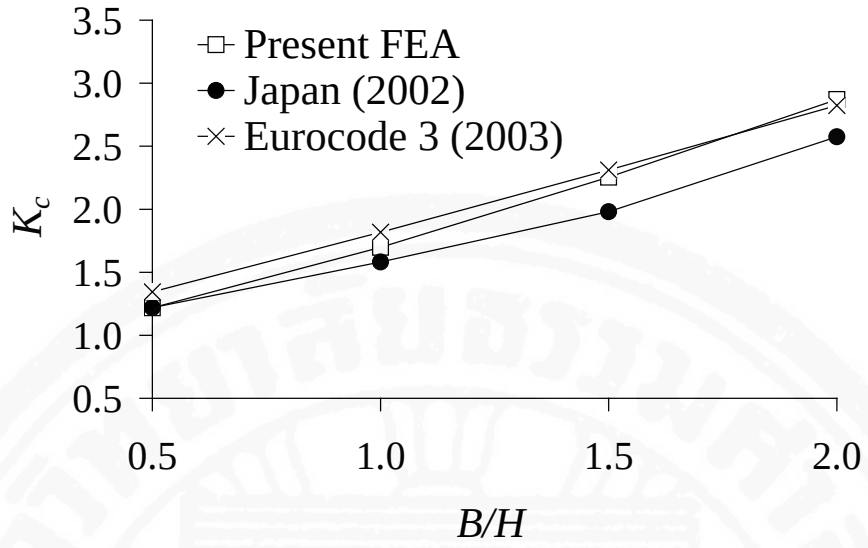

(b) Section B

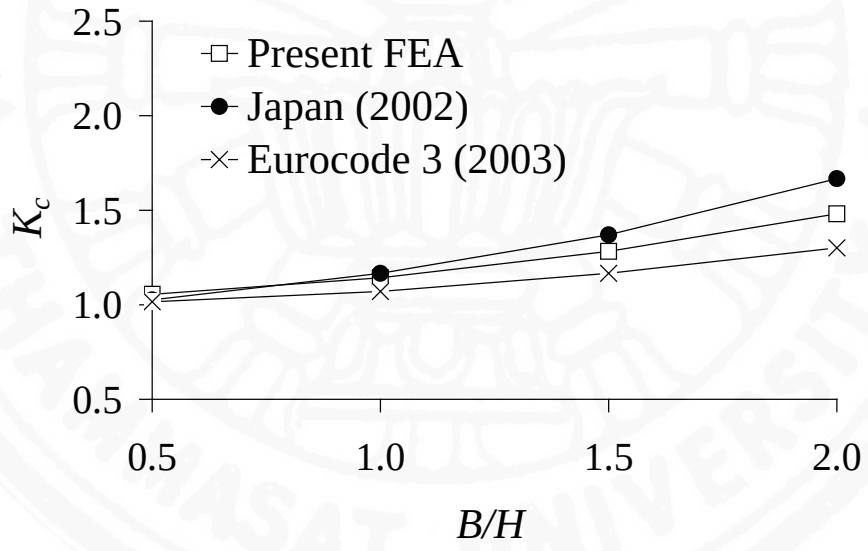

(c) Section C

Figure 4.8 Comparison of K_c values between cross sections varying with respect to B/H (H/L=0.1, T_f/T_w=1.0, α =1.25)

4.7 Empirical Formulas

4.7.1 Proposed Formulas

A data analysis program, Statistica of StatSoft, Inc., is used to conduct a regression analysis of the present FEA results, yielding the empirical formulas for K_c in the three sections of Section A to C. The empirical formulas thus obtained are presented in the following:

Section A:

$$K_c = (a_1)\left(\frac{B}{H}\right)^2 + (a_2)\left(\frac{B}{H}\right)\left(\frac{T_f}{T_w}\right) + \left[(a_3)\left(\frac{B}{H}\right) + (a_4)\left(\frac{T_f}{T_w}\right) + (a_5)\left(\frac{B}{H}\right)\left(\frac{T_f}{T_w}\right)\right](\alpha) + 1 \qquad (4.1)$$

where

$$a_1 = 6\left(\frac{H}{L}\right)^2 + \left(\frac{H}{L}\right) - 0.04$$

$$a_2 = -5\left(\frac{H}{L}\right)^2 - 1.7\left(\frac{H}{L}\right) + 0.07$$

$$a_3 = 3.5\left(\frac{H}{L}\right)^2 - \left(\frac{H}{L}\right) + 0.03$$

$$a_4 = -6\left(\frac{H}{L}\right)^2 + 0.7\left(\frac{H}{L}\right) - 0.01$$

$$a_5 = 15.2\left(\frac{H}{L}\right)^2 + 0.2\left(\frac{H}{L}\right) - 0.02$$

Section B:

$$K_c = (a_1)\left(\frac{B}{H}\right)^2 + (a_2)\left(\frac{B}{H}\right)\left(\frac{T_f}{T_w}\right) + \left[(a_3)\left(\frac{B}{H}\right) + (a_4)\left(\frac{T_f}{T_w}\right) + (a_5)\left(\frac{B}{H}\right)\left(\frac{T_f}{T_w}\right)\right](\alpha) + 1 \qquad (4.2)$$

where

$$a_1 = -4\left(\frac{H}{L}\right)^2 + 2.9\left(\frac{H}{L}\right)$$

$$a_2 = -15\left(\frac{H}{L}\right)^2 + 9.5\left(\frac{H}{L}\right) - 0.02$$

$$a_3 = -0.5\left(\frac{H}{L}\right)^2 + 0.76\left(\frac{H}{L}\right)$$

$$a_4 = -1.5\left(\frac{H}{L}\right)^2 - 0.3\left(\frac{H}{L}\right)$$

$$a_5 = 11\left(\frac{H}{L}\right)^2 - 4.9\left(\frac{H}{L}\right) + 0.03$$

Section C:

$$K_c = (a_1)\left(\frac{B}{H}\right) + (a_2)\left(\frac{T_f}{T_w}\right) + (a_3)\left(\frac{B}{H}\right)^2 (\alpha)^{-5} + (a_4) + 1 \tag{4.3}$$

where

$$a_1 = 10\left(\frac{H}{L}\right)^2 - 0.6\left(\frac{H}{L}\right) + 0.02$$

$$a_2 = 9\left(\frac{H}{L}\right)^2 - 0.6\left(\frac{H}{L}\right) + 0.02$$

$$a_3 = 18\left(\frac{H}{L}\right)^2 + 1.9\left(\frac{H}{L}\right) - 0.06$$

$$a_4 = -10\left(\frac{H}{L}\right)^2 + 0.4\left(\frac{H}{L}\right)$$

It is note that the above formulas are applicable for $0.025 \le \frac{H}{L} \le 0.2$, $0.5 \le \frac{B}{H} \le 2.0$, $0.5 \le \frac{T_f}{T_w} \le 2.0$ and $1.0 \le \alpha \le 1.5$.

4.7.2 Accuracy of the Proposed Formulas

Figure 4.9 illustrates some comparisons between the K_c values due to the empirical formulas and the present FEA. Good agreement is obvious in these figures. The overall accuracy of each proposed formula is calculated as the mean square error by the following equation:

$$\bar{\varepsilon} = \sqrt{\frac{1}{N}\sum_{i=1}^{N} \varepsilon_i^2} \tag{4.4}$$

where

$$\varepsilon_i = \frac{K_{cEmp} - K_{cFEA}}{K_{cFEA}} \times 100 \quad (\%) \tag{4.5}$$

N in Eq. (4.4) is the number of the present FEA results. $K_{c\ Emp}$ and $K_{c\ FEA}$ in Eq. (4.5) are the K_c values obtained from the proposed empirical formula and the present FEA, respectively. Since in the present study, the combination of the geometrical parameters has required 240 box girders to be analyzed, *N* is equal to 240. Using Eq. (4.4), the mean square error is found to be 3.0%, 2.9% and 4.2% for Sections A, B and C, respectively.

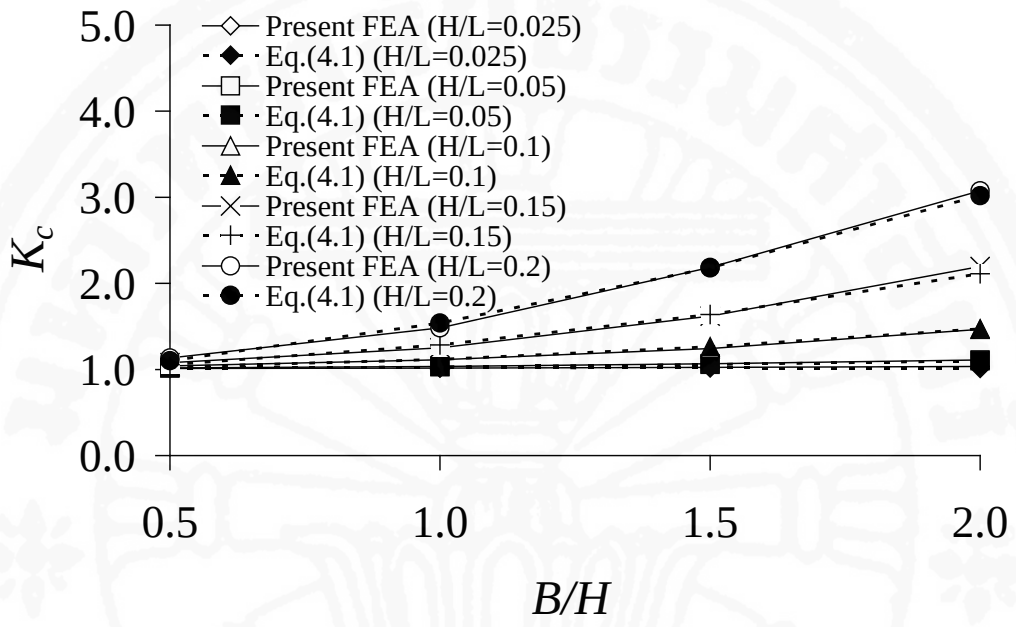

(a) Section A

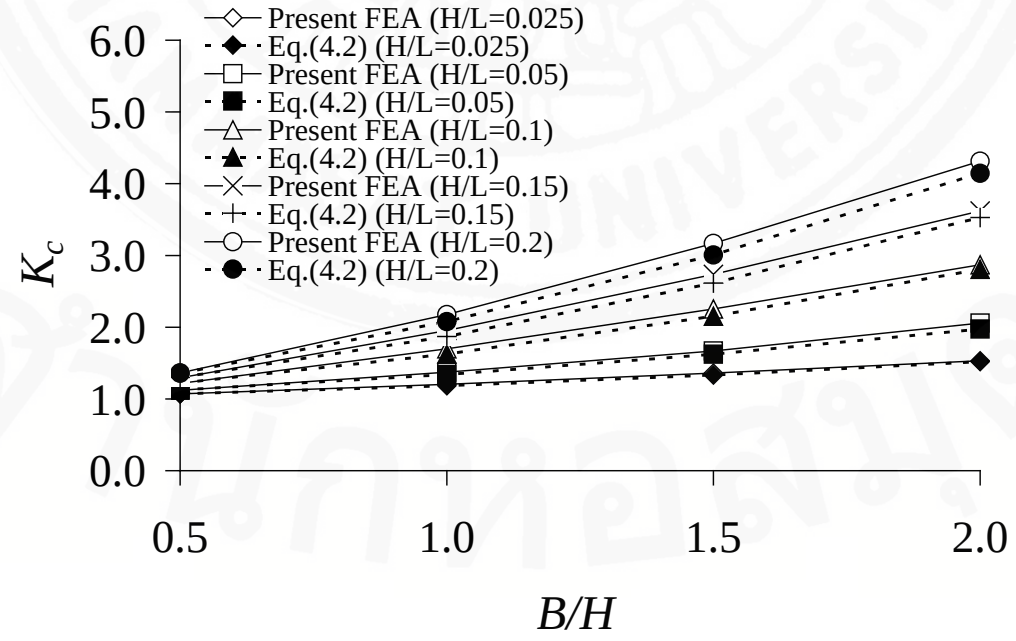

(b) Section B

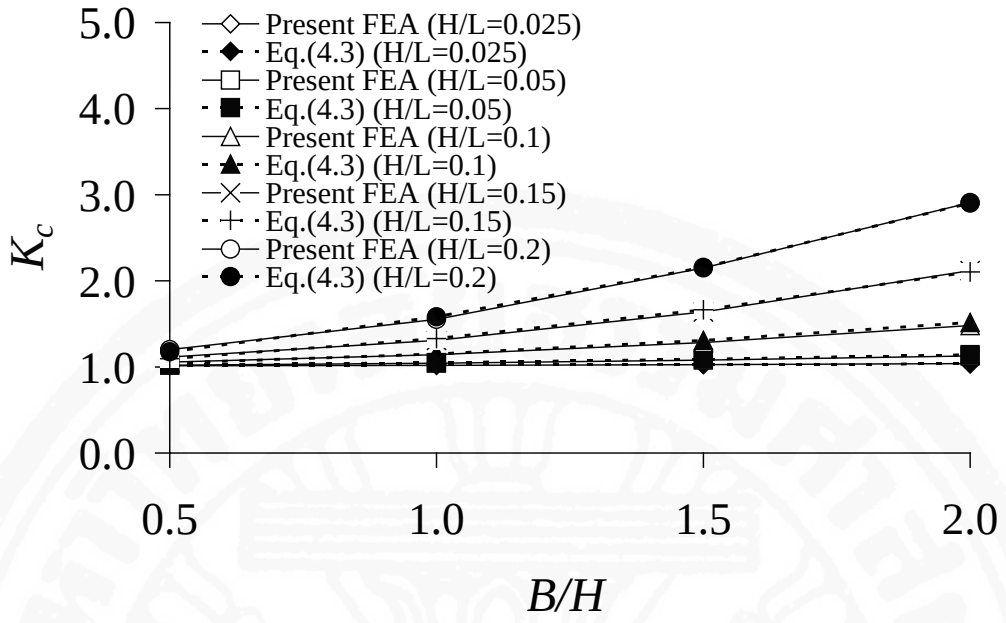

(c) Section C

Figure 4.9 K_c Comparison of K_c values due to proposed formulas and finite element analysis varying with respect to B/H (T_f/T_w=1.0, α =1.25)

4.8 Concluding Remarks

In this study, the three-dimensional finite element analysis of continuous box girders of various geometries has been performed so as to determine the shear lag effect in the continuous box girder on stress concentration. Shell elements have been used exclusively to model the entire box girder. The dependence of the stress concentration on the finite element mesh has been treated by the multimesh extrapolation method.

Based on the present numerical results thus obtained, empirical formulas have been proposed to compute the stress concentration factor K_c in three sections where large moments occur. It has been confirmed that the proposed formulas can yield the stress concentration factors in good agreement with the present finite element analysis results.